Inorganic Chemistry
Cite This: Inorg. Chem. 2018, 57, 2899−2907
Article
pubs.acs.org/IC

Periodic Trends in Actinyl Thio-Crown Ether Complexes

Shu-Xian Hu,[†,‡] Jing-Jing Liu,[‡] John K. Gibson,*[,§] and Jun Li*[,‡]

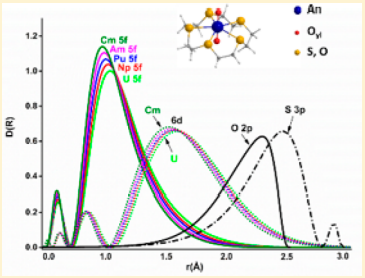
[†]Beijing Computational Science Research Center, Beijing 100193, China

[‡]Department of Chemistry and Key Laboratory of Organic Optoelectronics & Molecular Engineering of Ministry of Education, Tsinghua University, Beijing 100084, China

[§]Chemical Sciences Division, Lawrence Berkeley National Laboratory, Berkeley, California 94720, United States

Supporting Information

ABSTRACT: In-cavity complexes and their bonding features between thio-crown (TC) ethers and f-elements are unexplored so far. In this paper, actinyl(VI) (An = U, Np, Pu, Am, and Cm) complexes of TC ethers have been characterized using relativistic density functional theory. The TC ether ligands include tetrathio-12-crown-4 (12TC4), pentathio-15-crown-5 (15TC5), and hexathio-18-crown-6 (18TC6). On the basis of the calculations, it is found that the "double-decker" sandwich structure of $AnO_2(12TC4)_2^{2+}$ and "side-on" structure $AnO_2(12TC4)^{2+}$ are changed to "insertion" structures for $AnO_2(15TC5)^{2+}$ and $AnO_2(18TC6)^{2+}$ due to increased size of the TC ether ligands. The actinyl monocyclic TC ether complexes are found to exhibit conventional conformations, with typical $An-O_{actinyl}$ and $An-S_{ligand}$ distances and angles. Chemical bonding analyses by Weinhold's natural population analysis (NPA), natural localized molecular orbital (NLMO), and energy decomposed analysis (EDA), show that a typical ionic $An-S_{ligand}$ bond with the extent of covalent interaction between the An and S atoms primarily attributable to the degree of radial distribution of the S 3p atomic orbitals. The similarity and difference of the oxo-crown and TC ethers as ligands for actinide coordination chemistry are discussed. As soft S-donor ligands, TC ethers may be candidate ligands for actinide recognition and extraction.



1. INTRODUCTION

Actinide complexes are of both fundamental and practical interest, owing to their prevalence in the nuclear energy industry, which is an important source of electricity.[1−4] Therefore, issues related to nuclear fuel reprocessing and waste storage have to be addressed. Nuclear waste typically contains both actinides (mostly U, Np, Pu, Am, Cm) and their fission products (including lanthanides, Cs, and Tc) in an aqueous environment.[5] The treatment of nuclear waste, involving either separation of the actinides as useful commodities or their immobilization for long-term storage, is dominated by interactions with water.[6−9]

In aqueous solutions, uranium complexes exist mostly in the form of $U^{VI}O_2^{2+}$, whereas $Np^{VI}O_2^{2+}$ and $Pu^{VI}O_2^{2+}$ are substantially less stable relative to the reduced pentavalent actinyls $Np^{V}O_2^{+}$ and $Pu^{V}O_2^{+}$. $Am^{VI}O_2^{2+}$ is metastable.[10−14] Published structural data reveal a smooth actinide contraction of actinyl bond lengths, typically from R(U−O) = 1.80 Å to R(Am−O) = 1.75 Å.[15−18] The existence of CmO_2^{2+} in solution has not yet been reliably demonstrated, and this species is considered unimportant in curium chemistry due to the low stability of Cm(VI) in curinyl complexes.[19,20] The actinyl moiety is remarkable due to the fact that in contrast to similar d-element compounds it is linear and has very short metal−oxygen bond lengths suggesting strong multiple bond character. Actinyl complexes normally coordinate 4−6 monodentate ligands in their equatorial plane.[21−25] The f-elements, in contrast to many d-block transition metals, are in general hard acids and therefore have a strong affinity for hard O- and F-donor ligands. The choice of donor atoms has been a hot topic in the rational design of actinide separation or sequestering ligands.[26−28] It is well-known that actinides form somewhat more covalent bonds than lanthanides and therefore have slightly better affinities for soft bases such as S-donor ligands.[29] This could potentially be exploited in the separation of actinide from lanthanide cations.[30−32]

One of the methods proposed for nuclear waste treatment involves the coordination of actinide ions by polydentate macrocyclic ligands, thus exploiting the chelate effect.[33,34] Moreover, macrocyclic ligands could potentially be tuned to provide the best fit for specific cations and oxidation states by varying the size of the ligand's inner cavity.[35] There are many types of macrocyclic ligands known to date with much attention having been focused on N-donor ligands. Another important family of macrocyclic ligands are oxo-crown ethers and thio-crown (TC) ethers, the capacity of which to form stable complexes with transition metals is well-known.[36,37] Recently, several studies of crown ethers, both experimental and theoretical, have reported on the structural characterization,[38] the equatorial bonding properties of the actinyl cations, and bonding trends across the actinyl series.[7,39] However, in-cavity complexes and the corresponding bonding features between TC ethers and f-elements are essentially unexplored.

Theoretical studies on the factors determining the stability and bonding interactions between actinyls and TC ethers

Received: January 5, 2018
Published: February 19, 2018

Downloaded via LBRY FOR NATURAL SCIENCES RAS on August 23, 2018 at 07:34:04 (UTC).
See https://pubs.acs.org/sharingguidelines for options on how to legitimately share published articles.

© 2018 American Chemical Society

DOI: 10.1021/acs.inorgchem.7b03277
Inorg. Chem. 2018, 57, 2899−2907

could identify and rationalize the small covalency differences in bonding, and help in the development of new, more efficient separations processes. In this study, a series of $AnO_2(L)_n^{2+}$ (n = 1,2) complexes [An = U−Cm; L = tetrathio-12-crown-4 (12TC4), pentathio-15-crown-5 (15TC5), and hexathio-18-crown-6 (18TC6)] have been systematically explored using density functional theory (DFT). The structural parameters and their dependence on solvent interactions have been examined. The orbital interactions between actinyls and the coordinating ligands and the bonding trends across the series from An = U to An = Cm have been elucidated using various chemical bonding analysis approaches. Despite only UO_2^{2+} exhibiting a high stability, with the other AnO_2^{2+} (An = Np, Pu, Am, and Cm) likely being impractical candidates for actual separations processes, an evaluation of all six AnO_2^{2+} species provides a basis for a systematic comparative study and understanding of the stability and bonding trends.

2. METHODOLOGY

Quantum chemical calculations of the $AnO_2(L)_n^{2+}$ (An = U, Np, Pu, Am, and Cm; n = 1, 2; L = 12TC4, 15TC5, and 18TC6) complexes, their decomposed products, and the various ligands were carried out using spin-unrestricted Kohn−Sham DFT. The scalar relativistic DFT calculations were performed with the Gaussian 09[40] and ADF[41,42] for the geometry optimizations and vibrational frequency analyses. The geometry optimizations, Mulliken population analysis,[43] and the binding energy analysis were initially carried out using the local density approximation (LDA)[44] and generalized gradient approach (GGA) with PBE exchange-correlation functional[45] as implemented in ADF 2016.106. The scalar zeroth-order regular approximation (ZORA)[46,47] was used in conjunction with Slater type orbitals (STOs)[48] of the quality of triple-ζ plus polarization functions (TZP), and double-ζ plus polarization functions (DZP) for the valence electrons of the actinyls and TC ethers, respectively. The frozen core approximation was applied to the [$1s^2$−$5d^{10}$] cores of U, Np, Pu, Am, and Cm, the [$1s^2$] cores of C and O, and the [$1s^2$−$2p^6$] cores of S, with the rest of the electrons explicitly treated variationally. The geometry optimizations were performed without symmetry restrictions and were followed by vibrational frequency analysis to determine the local minima or saddle point natures of the optimized structures. The conductor-like screening solvation model (COSMO)[49] was employed to model the environment effect in crystals or to roughly consider the effects of water on the electronic and geometric structures of the complexes. The following atomic COSMO-default radii from the ADF code were used: U 2.100 Å, Np 2.100 Å, Pu 2.100 Å, Am 2.100 Å, Cm 2.100 Å, C 1.700 Å, S 1.792 Å, O 1.517 Å, and H 1.350 Å.[50] The reported reaction energies were obtained by combining the electronic energies with the zero-point vibrational energy corrections. The energy decomposition analyses (EDA)[51,52] and combined extended transition state (ETS)[53] with the natural orbitals for chemical valence (NOCV) theory were also carried out.[51,54,55] Bond order analyses were performed based on the Mayer method (BO_{Mayer})[56] and Nalewajski−Mrozek method (BO_{NM}).[54,55,57,58] The electron localization functions (ELF)[59] were calculated to investigate the features of the weak dative bonding.

In further geometry optimizations using Gaussian code, we used the scalar relativistic Stuttgart energy-consistent 32-valence-electron pseudopotential and associated ECP60MWB_SEG valence basis set[60−62] for the actinide atoms. The Dunning's correlation consistent basis set with polarized triple-ζ (cc-pVTZ)[63] were used for the oxygen, carbon, sulfur, and hydrogen atoms. The B3LYP hybrid density functional[64,65] was used in these calculations. The combination of these pseudopotentials and basis sets with this functional (labeled as B3LYP/ECP60MWB_SEG/cc-pVTZ level) has been shown to give accurate predictions of the properties and reaction energies of actinide complexes.[66,67] The Weinhold's natural bond orbitals (NBO)[68] and natural localized molecular orbital (NLMO)[69] analyses were performed at the B3LYP/6-31G* level[70] on optimized geometries from B3LYP calculations by using the NBO 5.0 program.[71]

3. RESULTS AND DISCUSSION

3.1. Structures and Stabilities of the $AnO_2(12TC4)^{2+}$ and $AnO_2(12TC4)_2^{2+}$. The theoretically optimized stable structures of the $AnO_2(12TC4)^{2+}$ and $AnO_2(12TC4)_2^{2+}$ (An = U, Np, Pu, Am, and Cm) complexes are shown in Figure 1; the structures

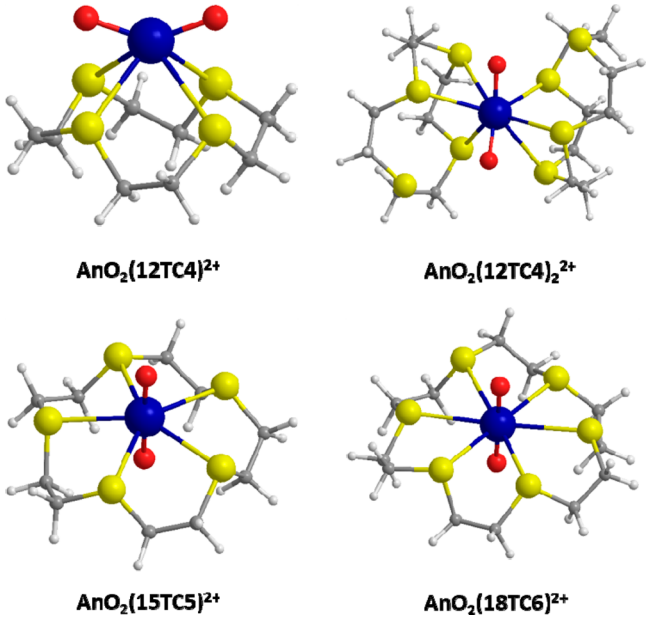


Figure 1. Optimized geometries of $AnO_2(12TC4)^{2+}$ (side-on), $AnO_2(12TC4)_2^{2+}$ (double decker), $AnO_2(15TC5)^{2+}$ (insertion), and $AnO_2(18TC6)^{2+}$ (insertion) using PBE/TZP/DZP. Selected parameters are listed in Table 1.

of the complexes for all five An elements are similar. The actinide metal center prefers coordination by the S atoms from one or both 12C4 in "side-on" or "double decker" structures rather than in-cavity "insertion" structures as identified below for other complexes. As apparent in Figure 1, the actinyl resides above the 12TC4 ligand in $AnO_2(12TC4)^{2+}$ and lies between two ligands in $AnO_2(12TC4)_2^{2+}$. These types of structures are usually rationalized as a misfit of actinyl cation and the inner cavity of a crown ether ligand, which is too small to accommodate alkali cations or the actinyl ions, which have similar effective ionic radii.[72,73]

In the "double decker" structure of $AnO_2(12TC4)_2^{2+}$ (Table 1), the actinyl (An = U, Np, and Pu) is coordinated by six crown ether S atoms (C_2 symmetry) from two 12TC4 (three S atoms of each ether) with An−S bond distances around 3.0 Å, which suggests weak bonding interactions. For smaller actinide atoms (An = Am and Cm), the coordination number is reduced from six to four. All the An−S bond lengths in the complexes are beyond the range of M−S covalent single-bond lengths estimated by the sum of the self-consistent covalent radii derived by Pyykkö,[74] indicating predominantly dative bonding. The calculated An−O distances decrease from uranium, where the U−O bond lengths are 1.796 Å, to plutonium, where the Pu−O bond lengths are 1.777 Å, and then increase to curium, where the Cm−O bond lengths are 1.812 Å. This plutonium turn phenomenon coincides with results for $[(AnO_2)(15C5)]^{2+}$ and $[(AnO_2)(CO_3)_3]^{4-}$ (An = U−Cm) and other actinide complexes in previous work.[3,7,23,75] The change in O−An−O bond angle from highly bent for U to linear for Am and Cm is due to gradually weaker bonding to the S atoms in 12TC4, as indicated by increasing An−S bond distance between the actinyl and TC ether from U to Cm, which was previously

DOI: 10.1021/acs.inorgchem.7b03277
Inorg. Chem. 2018, 57, 2899−2907

Table 1. Selected Average Bond Length (Å) and O≡An≡O Bond Angle (deg) of the Ground-State $AnO_2(12TC4)_2^{2+}$, $AnO_2(12TC4)^{2+}$, $AnO_2(15TC5)^{2+}$, and $AnO_2(18TC6)^{2+}$ in Vacuum and in Water Using COSMO Solvation Model (in Parentheses) at PBE/TZP/DZP Level[a]

			$AnO_2(12TC4)_2^{2+}$			$AnO_2(12TC4)^{2+}$			$AnO_2(15TC5)^{2+}$			$AnO_2(18TC6)^{2+}$		
			bond length		bond angle	bond length		bond angle	bond length		bond angle	bond length		bond angle
An	2S +1	elec. conf.	An≡O	An−S	O≡An≡O	An≡O	An−S	O≡An≡O	An≡O	An−S	O≡An≡O	An≡O	An−S	O≡An≡O
U	1	f^0	1.796 (1.799)	3.075 (3.067)	144.0 (147.8)	1.796	2.931, 3.069	139.4	1.778, 1.799 (1.786, 1.792)	2.931 (2.931)	180.0 (180.0)	1.781, 1.798 (1.791, 1.796)	3.090 (3.070)	180.0 (179.8)
Np	2	f_ϕ^1	1.793 (1.795)	3.024 (2.993)	151.6 (150.3)	1.787	2.932, 3.085	145.1	1.762, 1.782 (1.771, 1.776)	2.921 (2.921)	180.0 (179.9)	1.765, 1.782 (1.774, 1.780)	3.088 (3.070)	179.8 (179.6)
Pu	3	$f_\phi^1 f_\delta^1$	1.777 (1.779)	3.002 (2.991)	163.1 (161.6)	1.775	2.926, 3.279	159.9	1.761, 1.774 (1.766, 1.768)	2.915 (2.919)	180.0 (179.8)	1.761, 1.775 (1.766, 1.772)	3.080 (3.069)	179.3 (179.7)
Am	4	$f_\phi^1 f_\delta^2$	1.780 (1.777)	2.989 (2.958)	180.0 (179.0)	1.766	2.934, 3.994	177.8	1.756, 1.774 (1.763, 1.767)	2.906 (2.913)	180.0 (178.6)	1.760, 1.775 (1.767, 1.773)	3.098 (3.080)	179.8 (179.8)
Cm	5	$f_\phi^2 f_\delta^2$	1.812 (1.806)	3.022 (3.004)	180.0 (179.7)	1.794	2.894, 3.860	178.2	1.770, 1.779 (1.772, 1.775)	2.902 (2.904)	180.0 (180.0)	1.778, 1.798 (1.788, 1.797)	3.142 (3.131)	179.8 (179.9)

[a]The electron configurations are denoted using the quasi-atomic f^n configuration of actinides in an axial group, with f_σ, f_π, f_δ, and f_ϕ representing the orbitals from magnetic quantum numbers $m = 0, \pm1, \pm2, \pm3$, respectively.

discussed in the context of An−C distances in $(\eta^6\text{-}C_6H_3R_3)_2An$ complexes.[76]

In contrast to the "double decker" structures of the $An^{VI}O_2(12TC4)_2^{2+}$ complexes, in the "side-on" structure of $UO_2(12TC4)^{2+}$ the uranyl is coordinated to all four S atoms of one 12TC4 (C_2 symmetry) with U−S bond lengths of 2.931 and 3.069 Å (Table 1). Notably, the An coordination number decreases from four in $UO_2(12TC4)^{2+}$ to two in $CmO_2(12TC4)^{2+}$ with average An−S distances increasing from 3.000 to 3.377 Å, likely due to decreasing charge and contraction of the 5f/6d orbitals resulting in weaker bonding from U to Cm. The calculated An−O distances decrease from uranium, where the U−O bond lengths are 1.796 Å, to americium, where the Am−O bond lengths are 1.766 Å, as expected based on the decrease in ionic radii across the series. The distance increases for curium to Cm−O bond lengths of 1.794 Å, as expected due to the decrease of ionic and covalent bonding.[23] A substantial energy of ∼60 kcal/mol (Table 2) is released upon binding of $An^{VI}O_2(12TC4)^{2+}$ to another 12TC4 ether to form $An^{VI}O_2(12TC4)_2^{2+}$. The initial $An^{VI}O_2(12TC4)^{2+}$ complex can be considered as an intermediate along the reaction path of $An^{VI}O_2^{2+} + 2(12TC4) \rightarrow An^{VI}O_2(12TC4)_2^{2+}$; the electronic structure and bonding feature discussions for $An^{VI}O_2(12TC4)^{2+}$ are not presented in the main text but can be found in the Supporting Information.

Because these f-element complexes are predominantly ionic, and nuclear fuel reprocessing is usually in aqueous solutions, polarized solvation effects of water by using the COSMO model were roughly assessed for the geometrical structures of the $AnO_2(12TC4)_2^{2+}$ (An = U, Np, Pu, Am, and Cm) complexes. Since solvation minimally affects the coordination and gives essentially the same structure trends, the following computational decomposition of the bonding was performed in the gas phase. In addition to ionic interactions between ligands and the actinyl (VI) cations, some insights are presented for charge transfer and polarization effects.

3.2. Structures and Stabilities of the $AnO_2(15TC5)^{2+}$.

The geometrical optimization for the $An^{VI}O_2(15TC5)^{2+}$ and $An^{VI}O_2(15TC5)_2^{2+}$ (An = U, Np, Pu, Am, and Cm) complexes have been explored. In contrast to the 12TC4 complexes, the insertion structures of $An^{VI}O_2(15TC5)^{2+}$ are stable. The $An^{VI}O_2(15TC5)_2^{2+}$ are unstable with large imaginary frequencies, leading to the formation of the $An^{VI}O_2(15TC5)^{2+}$ shown in Figure 1. AnO_2^{2+} complexes prefer adopting either a pseudoplanar penta- or hexa-coordinate structure, as provided by a 15TC5 or a 18TC6 ligand, respectively;[77] this is the inherent reason that the doubly ligated complexes are relatively unstable. The $An^{VI}O_2^{2+}$ prefer coordination by one rather than two 15TC5; this is considered as due to a weak bonding interaction of metal and sulfur atoms, large steric repulsion between two 15TC5 ligands and the ability of the actinyls to insert into the larger 15TC5 to achieve penta-coordination. In contrast to the "side-on" structure of $AnO_2(12TC4)^{2+}$ or "double decker" structure of $AnO_2(12TC4)_2^{2+}$, the ground-state structures of the $AnO_2(15TC5)^{2+}$ feature an "insertion" mode, in which the actinyl stands inside the cavity of the TC ether and coordinates to all five S atoms with the average An−S distance decreasing from 2.931 Å for An = U to 2.902 Å for An = Cm (Table 1). This variation is partially attributed to the relativistic and nuclear-shielding contraction of the An ionic radius. As was found for our previously studied oxo-crown complex, $An^{VI}O_2(15C5)^{2+}$ (An = U, Np, Pu, Am, and Cm),[39] the AnO_2^{2+} is similarly trapped in the center of 15TC5 with an

DOI: 10.1021/acs.inorgchem.7b03277
Inorg. Chem. 2018, 57, 2899−2907

Table 2. Binding Energy (BE, kcal/mol) Defined as $AnO_2^{2+} + nL \rightarrow AnO_2(L)_n^{2+}$ (L = 12TC4, n = 1 and 2; L= 15TC5, 18TC6, n = 1) at PBE/TZP/DZP Level with Scalar Relativistic (SR) and Spin−Orbit (SO) Coupling Corrections

			$AnO_2(12TC4)^{2+}$		$AnO_2(12TC4)_2^{2+}$		$AnO_2(15TC5)^{2+}$		$AnO_2(18TC6)^{2+}$	
An	2S+1	elec. conf.	SR	SO	SR	SO	SR	SO	SR	SO
U	1	f^0	−198.7	−200.7	−270.0	−272.1	−245.3	−251.1	−265.3	−271.6
Np	2	f_ϕ^1	−198.6	−198.5	−267.4	−267.7	−241.3	−245.6	−260.8	−265.0
Pu	3	$f_\phi^1 f_\delta^1$	−195.2	−193.5	−263.9	−262.7	−245.5	−249.0	−262.4	−266.0
Am	4	$f_\phi^1 f_\delta^2$	−193.8	−192.0	−266.1	−264.6	−242.8	−245.7	−266.2	−267.2
Cm	5	$f_\phi^2 f_\delta^2$	−182.3	−187.9	−256.0	−260.0	−232.1	−239.8	−243.9	−251.7

An−S distance of 2.9 Å; this is substantially longer than the An−O dative bond length of 2.4 Å, which is a result of the larger atomic/ionic radii and lower electronegativity of S compared to O.[39] The calculated An−O_{yl} distances in $AnO_2(15TC5)^{2+}$ decrease from uranium (average U−O_{yl} distance ≈1.789 Å) to americium (average Am−O_{yl} distance ≈1.765 Å), then increase up to curium (average Cm−O_{yl} distance ≈1.765 Å), due to the balance between the contraction in atomic radii and the reduced charge interaction and orbital overlap. The AnO_2^{2+} bonding trend appears consistent with that in $AnO_2(12TC4)^{2+}$ and is different from what was previously observed in the $AnO_2(15C5)^{2+}$ (An = U−Cm) complexes, for which an unusually short Am−O_{yl} bond was found and attributed to enhanced orbital overlap interaction in the Am−O_{yl} vs Pu−O_{yl} bond. Additionally, the magnitude of decreasing An−O_{yl} distances is consistent with the actinide contraction across the 5f series upon moving from U to Pu, but is slightly larger than expected from Pu to Am.[78]

3.3. Structures and Stabilities of the $AnO_2(18TC6)^{2+}$.

As for 15TC5, $An^{VI}O_2(18TC6)_2^{2+}$ is unstable relative to decomposition to $An^{VI}O_2(18TC6)^{2+}$ and 18TC6. The optimized structures of the $An^{VI}O_2(18TC6)^{2+}$ (An = U, Np, Pu, Am, and Cm) complexes are similar and displayed in Figure 1. The An−S distances are longer than 3.0 Å (Table 1), indicating a weaker interaction between An and S_{18TC6} than that between An and S_{15TC5}, which is confirmed from average Mayer bond order value of 0.3 and 0.4 for An−S_{18TC6} and An−S_{15TC5}, respectively. The turning-point of An−O_{yl} bond lengths occurs at An = Am, in agreement with the above results for $An^{VI}O_2(12C4)^{2+}$ and $An^{VI}O_2(15TC5)^{2+}$, and shifted up from the plutonium turn in the oxo-crown complexes, which is consistent with the appearance of the turn at AmO_2^{2+} in isolated actinyls (Table 3), indicating a relatively weaker ligand field effect on $An^{VI}O_2^{2+}$ of the TC sulfur versus the crown oxygen.

The structural results indicate that the average metal−ligand distances increase in the order An−S_{12TC4} > An−S_{15TC5} < An−S_{18TC6}. The fact that the An−S_{15TC5} bond lengths are shorter than those of An−S_{18TC6} is due to the smaller cavity radius of 15TC5 ether. The shorter An−S_{15TC5} bond length compared with An−S_{12TC4} can be partially ascribed to their different coordination structures. Surprisingly, while the An−S bonds appeared to follow the actinide contraction consistent with ionic interactions strengthening from U to Cm, an unexpectedly long Cm−S_{12TC4} and Cm−S_{18TC6} bond was found and attributed to the low stability of $Cm^{VI}O_2^{2+}$ TC ether complexes with the unstable Cm^{VI} oxidation state. This decrease-then-increase trend of An−L bond distances from U to Cm is consistent with our previous findings in other complexes with plutonium turn phenomenon.[23] As seen in Table 4, the increasing spin density of actinides provides evidence for the instability of $Cm^{VI}O_2^{2+}$ and the turn-point of bond length at plutonium in $AnO_2(12TC4)_2^{2+}$ and at americium in $AnO_2(15TC5)^{2+}$ and $AnO_2(18TC6)^{2+}$.

Table 3. An−O Bond Length (Å) of Isolated AnO_2^{2+} at Different Exchange-Correlation Functionals Along with T2ZP Basis Set for All Atoms

	LDA	PBE	PBE0	HF[a]	SO-CASPT2[79]
U	1.700	1.716	1.686	1.654	1.710
Np	1.698	1.714	1.679	1.641	1.700
Pu	1.685	1.703	1.666	1.627	1.675
Am	1.675	1.695	1.652	1.649	1.679
Cm	1.687	1.712	1.674	1.989	1.674

[a]HF denotes *ab initio* Hartree−Fock methods in the wave function theory.

3.4. Electronic Structure and Bonding Analyses of $AnO_2^{2+}(L)_n$.

Insights into the involvement of the actinide 5f orbitals in bonding were obtained through electronic structure analyses of the $AnO_2(15TC5)^{2+}$ at the B3LYP/TZ2P level. Selected Kohn−Sham molecular orbitals in the HOMO−LUMO region involving the 5f orbitals are depicted in Figure 2 as the energy levels of 5f-, 6d-, and 7s-based MOs of the actinide fragments together with the S 3p orbitals. The MOs from the S 3p are fully occupied, and the highest singly occupied α spin orbitals (SOMOs) are occupied in An. The An 6d and An 7s AOs slightly increase in energy from U to Cm, while the 5f orbitals significantly decrease in energy so that they become nearly degenerate with the sulfur lone-pair orbitals at around plutonium. The An 5f orbitals are stabilized so much so that they eventually lie below the ligand orbitals beyond Am. This is a general feature of actinide chemistry, which has been observed in a number of actinide complexes with different ligands.[3,23,75] Although the best energy match of the 5f- and S-based orbitals occurs for Pu

Table 4. Mulliken and Multipole Derived Charge (MDC) Spin Density of An in AnO_2^{2+}, $AnO_2(12TC4)_2^{2+}$, $AnO_2(15TC5)^{2+}$, and $AnO_2(18TC6)^{2+}$ (An = U, Np, Pu, Am, and Cm) at the SR−PBE/TZ2P Level

		AnO_2^{2+}		$AnO_2(12TC4)_2^{2+}$		$AnO_2(15TC5)^{2+}$		$AnO_2(18TC6)^{2+}$	
species	spin	MDC-q	Mulliken	MDC-q	Mulliken	MDC-q	Mulliken	MDC-q	Mulliken
U	0	0.00	0.00	0.00	0.00	0.00	0.00	0.00	0.00
Np	1	1.18	1.12	1.27	1.46	1.01	1.22	1.07	1.31
Pu	2	2.17	2.27	2.48	2.84	2.08	2.48	2.14	2.57
Am	3	3.46	3.44	4.02	4.45	3.17	3.79	3.36	4.02
Cm	4	4.76	4.70	4.73	5.29	4.05	4.82	4.21	4.97

DOI: 10.1021/acs.inorgchem.7b03277
Inorg. Chem. 2018, 57, 2899−2907

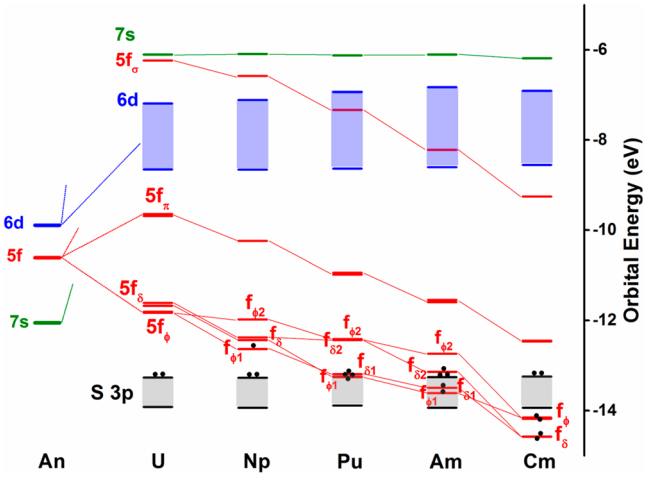


Figure 2. Scalar relativistic KS-PBE molecular orbital energy levels of free $AnO_2(15TC5)^{2+}$ ions for An = U, Np, Pu, Am, and Cm. The ground valence electronic configuration for isolated NpO_2^{2+}, PuO_2^{2+}, AmO_2^{2+}, and CmO_2^{2+} are $1\phi_u^1 1\delta_u^0$, $1\phi_u^1 1\delta_u^1$, $1\phi_u^1 1\delta_u^2$, and $1\delta_u^2 1\phi_u^2$, respectively. Gray column: sets of highest occupied S 3p type MOs. The blue column: the sets of empty An 6d type MOs.

and Am, poor spatial overlap due to a An−S distance of larger than 3.0 Å suggests that this result should not be interpreted as an indication of an increased covalent bonding interaction. In contrast to the significant orbital mixing at An = Am with oxygen ligands, An 5f and S 3p AOs mix strongly due to the higher energy level of S 3p AOs than that of O 2p.

Beside the wave function-based chemical bonding analyses, the ETS-NOCV analysis (Table 5) was carried out in order to reveal the intrinsic bonding mechanism in terms of the major energy contributions to the orbital interactions. The degree of ionicity and covalency of the An−S_L bond in $AnO_2(L)^{2+}$ (An = U, Np, Pu, Am, and Cm) has been evaluated by a quantitative index. The trend of covalent character from U to Cm in all the studied complexes can be understood in terms of both the energy degeneracy of S 3p and An 5f AOs, and the extent of radial distribution of S 3p AOs that favors large orbital overlap, which contributes to a considerable energetic stabilization as seen in Table 2.[75,80] In contrast to the covalency, the ionic character for these complexes has an opposite trend of decreasing from U to Cm, due to the reduced charge density of the actinides from U to Cm for all studied species, as shown in Figure 3. Thus, the chemical bonding between the actinyl and

Table 5. EDA and ETS-NOCV Analysis of $AnO_2(12TC4)_2^{2+}$, $AnO_2(15TC5)^{2+}$, and $AnO_2(18TC6)^{2+}$ (An = U, Np, Pu, Am, and Cm) Complexes according to Two Fragments of AnO_2^{2+} and Ligands $(12TC4)_2$, 15TC5, and 18TC6 at PBE/TZ2P Level of theory

	Pauli repulsion	electrostatic interaction	orbital interactions	interaction energy	OI%[a]
		$AnO_2(12TC4)_2^{2+}$			
U	182.3	−193.1	−242.3	−253.0	0.56
Np	165.9	−189.5	−260.4	−284.1	0.58
Pu	140.9	−176.6	−259.8	−295.5	0.60
Am	136.5	−172.3	−304.0	−339.8	0.64
Cm	141.1	−179.1	−317.4	−355.5	0.64
		$AnO_2(15TC5)^{2+}$			
U	213.0	−210.8	−255.0	−252.9	0.55
Np	206.8	−208.8	−253.8	−255.8	0.55
Pu	199.4	−206.2	−281.6	−288.4	0.58
Am	193.8	−201.7	−304.1	−312.0	0.60
Cm	187.0	−201.8	−325.3	−340.1	0.62
		$AnO_2(18TC6)^{2+}$			
U	133.9	−171.4	−243.4	−281.0	0.59
Np	127.4	−168.5	−270.0	−311.1	0.62
Pu	123.8	−166.9	−267.9	−311.0	0.62
Am	112.0	−161.1	−312.1	−361.2	0.66
Cm	111.7	−159.8	−307.4	−355.5	0.66

[a]OI% = E[orbital interactions]/(E[orbital interactions] + E[electrostatic interaction]).

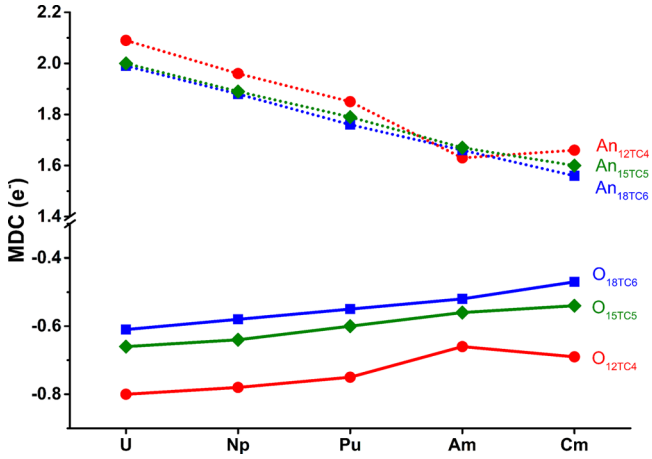


Figure 3. Plot of average multipole derived charges (MDC) of $AnO_2(12TC4)_2^{2+}$, $AnO_2(15TC5)^{2+}$, and $AnO_2(18TC6)^{2+}$ (An = U, Np, Pu, Am, and Cm) at the SR−PBE/TZ2P level.

TC ether ligands features a turning-point at An = Pu or Am, as a result of balancing between the decreasing ionic dative bonding and the somewhat increasing covalent interaction. Irrespective of the structure and the actinide, the An 5f/6d orbitals are mainly localized on the actinide site (see the plot of representative An−S_L bonding interaction from ETS-NOCV method in Figures S1−S3). There is little evidence for interaction of the An 5f orbitals with any coordinating sulfur atoms of the TC ether ligands. Additional electron localization function (ELF, Figures S4−S6) analyses reveals that despite that the An−S_L bonds being primarily centered on the An and S_L atoms the An−S_L dative bonds possess primarily ionic character.

A comprehensive assessment of the structure and bonding of these complexes was performed. The average bond distances (Tables S7−S10), average Mayer bond orders (Tables S7−S10), average Mulliken charges (Table S11) and average Hirshfeld charges[81] (Table S12), and average multipole derived charges[82] (Table S13) of the $AnO_2(12TC4)_2^{2+}$, $AnO_2(15TC5)^{2+}$ and $AnO_2(18TC6)^{2+}$ complexes were calculated with PBE ZORA/TZ2P. The mean An−O bond distance vs An−O bond order and An−S bond distance vs An−S bond order are presented in Figure 4. The Mayer bond order shows An−O orders higher than 2, in good agreement with the generally accepted view that these An−oxo bonds in actinyls possess partial triple bond character. Although some triple bond character remains, reduction of the actinyl oxidation state from +VI to +V for An = U−Cm decreases the corresponding bond orders because the extra electron occupies a nonbonding f-orbital or partially antibonding orbitals due to the energy levels of the 5f-orbitals lying close to or even below those of the O 2p orbitals. The Mayer bond orders for bonds between actinides and the equatorial sulfur

DOI: 10.1021/acs.inorgchem.7b03277
Inorg. Chem. 2018, 57, 2899−2907

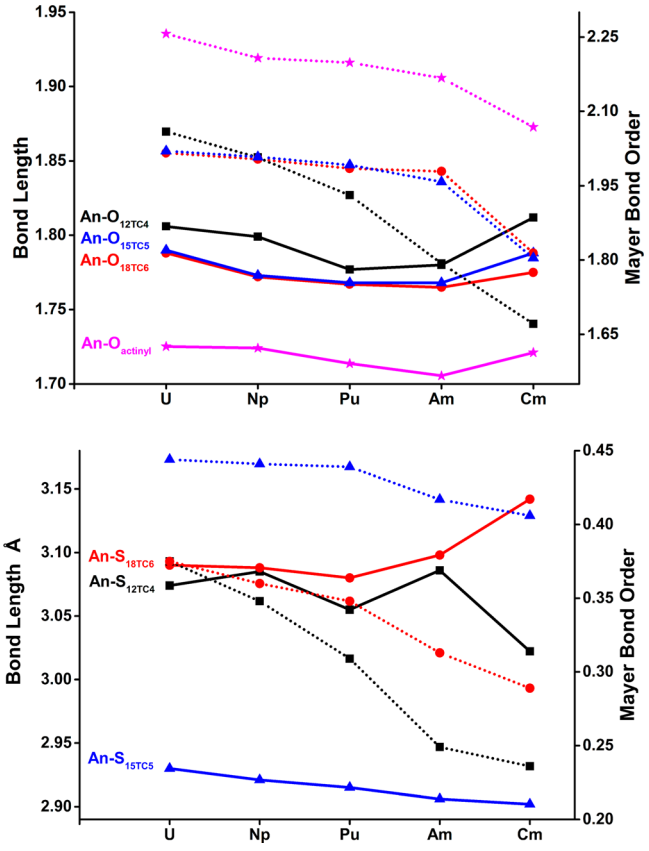


Figure 4. Top: mean An−O bond distance (solid lines, left axis) and An−O bond order (dotted lines, right axis) of isolated AnO_2^{2+} (pink stars), $AnO_2(12TC4)_2^{2+}$ (black squares), $AnO_2(15TC5)^{2+}$ (blue triangles), and $AnO_2(18TC6)^{2+}$ (red circles). Bottom: mean An−S bond distance (solid lines, left axis) and An−S bond order (dotted lines, right axis) of $AnO_2(12TC4)_2^{2+}$ (black squares), $AnO_2(15TC5)^{2+}$ (blue triangles), and $AnO_2(18TC6)^{2+}$ (red circles).

ligands are substantially less than 1, with a bond order trend of $An-S_{12TC4} > An-S_{15TC5} > An-S_{18TC6}$ attributed to the longer bond distances from 12TC4 to 18TC6. However, the complexes of actinyls with 15TC5 and 18TC6 have higher bond orders ($U-S_{15TC5}$ bond orders of 0.44, $U-S_{18TC6}$ bond orders of 0.38) than those complexes of actinyl with 15-crown-5 ($U-O_{eq}$ bond orders of 0.36)[39] and 18-crown-6 ($U-O_{eq}$ bond orders of 0.33),[83] due to the large extended radial distribution of the S 3p orbitals compared with the rather contracted O 2p orbitals. Of particular importance is the trend that upon proceeding across the actinide series the $An-S_L$ bond orders and total binding energies generally decrease in parallel with a decrease in the electrostatic interaction. This trend further confirms that the reduced distance of the $An-S_L$ bonds from An = U to Cm does not result in stronger bonding because the $An-S_L$ bonds are dominated by ionic bonding that gradually decreases from An = U to Cm.

Further insights into the electronic structure of the actinyl TC ether complexes were obtained from natural localized molecular orbital (NLMO) analyses, the results of which are given in Table S10. The calculated NLMO results show that the TC ether ligand has p-type lone pairs on the ether sulfur atoms, similar to the oxygen atoms of the 15-crown-5 ligand as shown in our previous work.[39] Upon coordination to AnO_2^{2+}, the $An-S_L$ interactions are mainly ionic, with rather weak $An-S_L$ covalent interactions that feature a decreasing trend of $\sigma_{S12TC4\text{-}An}$ bonding in the equatorial plane.

3.5. Comparison of $AnO_2(15C5)^{2+}$ and $AnO_2(15TC5)^{2+}$.

Extensive theoretical studies were carried out to understand the similarities in chemical bonding between $An-O_{ligand}$ in $AnO_2(15C5)^{2+}$ and An−S in $AnO_2(15TC5)^{2+}$ (selected geometrical parameters in Figure 5). The relatively longer average

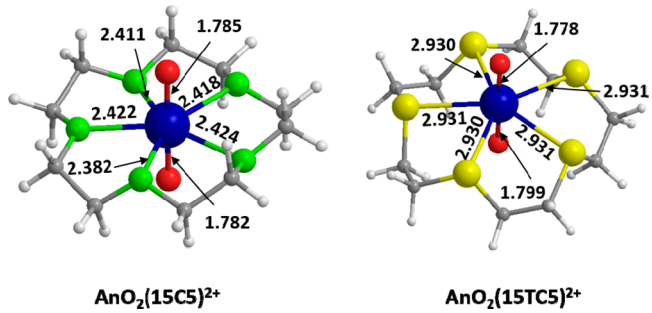


Figure 5. Computed structures of the ground-state $[UO_2(15C5)]^{2+}$ and $[UO_2(15TC5)]^{2+}$ complexes. Selected geometrical parameters are shown. The uranyl O atoms are red while the crown ether O atoms are green. The $U-O_{yl}$ distance is ~0.02 shorter in $[UO_2(15C5)]^{2+}$ than that in $[UO_2(15TC5)]^{2+}$ complex, implying more reactive uranyl in the latter.

bond length of An−S (2.93 Å) in $AnO_2(15TC5)^{2+}$ versus that of $An-O_{ligand}$ (2.41 Å)[39] in $AnO_2(15C5)^{2+}$ reveals weaker ionic bonding in the 15TC5 complexes due to reduced ionic charges on the atoms. Because the electrostatic interaction (E_{elstat}) is inversely proportional to the metal−ligand distances, this result is consistent with the E_{elstat} values of −193.1 kcal/mol for $UO_2(15TC5)^{2+}$ and −250.3 kcal/mol for $UO_2(15C5)^{2+}$.[39] In addition to the ionic interaction, the bonding trend can be perturbed by the dative stabilization due to covalent An−ligand overlap interaction, which is directly attributed to the degree of An(d,f)−O(2p)/S(3p) overlap. Referring to the radial atomic orbital (AO) density plots in Figure 6, it is apparent that the An

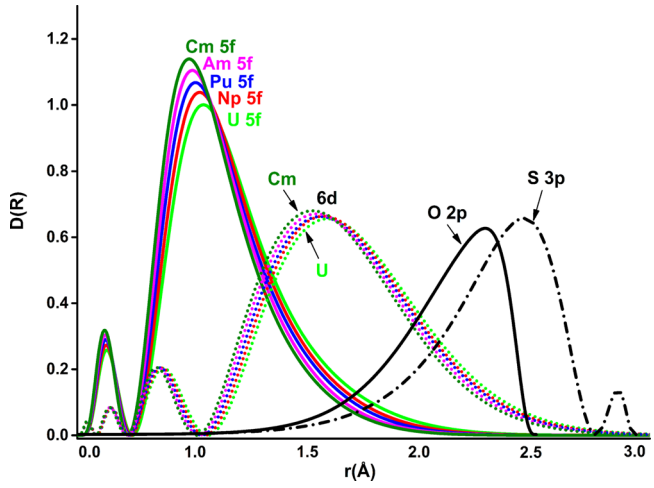


Figure 6. Atomic valence orbital radial densities $D(r) = r^2 R(r)^2$ of 5f (solid line) and 6d (dotted line) orbitals of the atomic ions $U^{6+}-Cm^{6+}$ from B3LYP density functional calculations. The overlap of the radial orbital densities of O 2p (black solid line) and of S 3p (black dashed line) are centered at typical distances of weakly bonded O at 2.4 Å from An and weakly bonded S at 3.0 Å, respectively.

5f6d hybrid AOs effectively overlap with S 3p orbitals, with the overlap being the best for U and decreasing slightly to Cm. Because of the much more extended radial distribution of the S(3p) AOs, the S(3p)−An(d,f) overlap extends to a substantially

DOI: 10.1021/acs.inorgchem.7b03277
Inorg. Chem. 2018, 57, 2899−2907

longer range compared to that of the O(2p)−An(d,f) overlap. These model results emphasize that sulfur considered as a relatively soft ligand should generally be useful in the design of new more efficient separation extractants.

4. CONCLUSIONS

We have investigated the electronic and geometric structures of complexes formed between actinyls AnO_2^{2+} (An = U−Cm) and TC ether macrocyclic ligands using different quantum chemical methods. The agreement between the different approaches, as well as comparison with available experimental data (such as geometries, vibrational frequencies, and reduction potentials) confirms the validity and accuracy of the methodology. Our evaluation of the coordination chemistry of actinyls with TC ethers provides the following guidance: (1) The cavity of 12-thio-crown-4 ether is too small to accommodate actinyl ions, while AnO_2^{2+} fit well into 5-thio-crown-5 ether and 18-thio-crown-6 ether to form a 5- or 6-fold coordinated An−S_L ionic bonds in the equatorial plane. (2) All the complexes formed by these ligands possess distorted geometries with a twist-like conformation of the ligand macrocycle. (3) An−S_L dative bonding is rather weak, and the change in the bond order is in the orderings of 15TC5 > 18TC6 and U > Np > Pu > Am > Cm. (4) The relatively weak interactions and small changes in chemical bonding indicate a complicated nature of An−S interactions that is necessary to fully understand for the design of potential new S-ligand extractants. The current study of the actinide complexes with thio-crown-ether ligands helps to provide insights for design soft-donor ligands for actinide-actinide and actinide-lanthanide separations.

■ ASSOCIATED CONTENT

Supporting Information

The Supporting Information is available free of charge on the ACS Publications website at DOI: 10.1021/acs.inorgchem.7b03277.

(PDF)

■ AUTHOR INFORMATION

Corresponding Authors

*E-mail: jkgibson@lbl.gov.
*E-mail: junli@tsinghua.edu.cn.

ORCID

John K. Gibson: 0000-0003-2107-5418
Jun Li: 0000-0002-8456-3980

Notes

The authors declare no competing financial interest.

■ ACKNOWLEDGMENTS

This work was supported by the Science Challenge Project (JCKY2016212A504), the National Natural Science Foundation of China (grant no. 21433005, 91426302, 21590792, and 21701006) and NSAF (U1530401) the Foundation of President of China Academy of Engineering Physics (No. YZJJSQ2017072) [J.L. and S.X.H], and as part of the Center for Actinide Science and Technology (CAST) an Energy Frontier Research Center (EFRC) funded by the U.S. Department of Energy (DOE), Office of Science, Basic Energy Sciences (BES), under Award Number DE-SC0016568 [J.K.G.].

■ REFERENCES

(1) Morss, L. R., Edelstein, N. M., Fuger, J., Eds. *The Chemistry of the Actinide and Transactinide Elements*; 3rd ed.; Springer: Dordrecht, The Netherlands, 2006; Vols. *1 and 2*.

(2) Kubicki, J. D.; Halada, G. P.; Jha, P.; Phillips, B. L. Quantum mechanical calculation of aqueuous uranium complexes: carbonate, phosphate, organic and biomolecular species. *Chem. Cent. J.* **2009**, *3* (10), 1−29.

(3) Li, J.; Bursten, B. E. Electronic structure of cycloheptatrienyl sandwich compounds of actinides: An(η^7-C_7H_7)$_2$ (An = Th, Pa, U, Np, Pu, Am). *J. Am. Chem. Soc.* **1997**, *119* (38), 9021−9032.

(4) Kelley, M. P.; Su, J.; Urban, M.; Luckey, M.; Batista, E. R.; Yang, P.; Shafer, J. C. On the origin of covalent bonding in heavy actinides. *J. Am. Chem. Soc.* **2017**, *139* (29), 9901−9908.

(5) Kaltsoyannis, N. Does covalency increase or decrease across the actinide series? Implications for minor actinide partitioning. *Inorg. Chem.* **2013**, *52* (7), 3407−3413.

(6) Lucena, A. F.; Odoh, S. O.; Zhao, J.; Marcalo, J.; Schreckenbach, G.; Gibson, J. K. Oxo-Exchange of Gas-Phase Uranyl, Neptunyl, and Plutonyl with Water and Methanol. *Inorg. Chem.* **2014**, *53* (4), 2163−2170.

(7) Hu, S. X.; Gibson, J. K.; Li, W. L.; Van Stipdonk, M. J.; Martens, J.; Berden, G.; Redlich, B.; Oomens, J.; Li, J. Electronic structure and characterization of a uranyl di-15-crown-5 complex with an unprecedented sandwich structure. *Chem. Commun.* **2016**, *52* (86), 12761−12764.

(8) (a) Su, J.; Schwarz, W. H. E.; Li, J. Electronic spectra and excited states of neptunyl and its $NpO_2Cl_4^{2-}$ complex. *Inorg. Chem.* **2012**, *51* (5), 3231−3238. (b) Su, J.; Wang, Z.-M.; Pan, D.-Q.; Li, J. Excited States and Luminescent Properties of UO_2F_2 and Its Solvated Complexes in Aqueous Solution. *Inorg. Chem.* **2014**, *53* (14), 7340−7350.

(9) Vidaud, C.; Bourgeois, D.; Meyer, D. Bone as target organ for metals: The case of f-elements. *Chem. Res. Toxicol.* **2012**, *25* (6), 1161−1175.

(10) Yang, X.; Chai, Z. F.; Wang, D. Q. Theoretical investigation on the mechanism and dynamics of oxo exchange of neptunyl(VI) hydroxide in aqueous solution. *Phys. Chem. Chem. Phys.* **2015**, *17* (11), 7537−7547.

(11) (a) Su, J.; Dau, P. D.; Qiu, Y. H.; Liu, H. T.; Xu, C. F.; Huang, D. L.; Wang, L. S.; Li, J. Probing the electronic structure and chemical bonding in tricoordinate uranyl complexes $UO_2X_3^-$ (X = F, Cl, Br, I): competition between Coulomb repulsion and U-X bonding. *Inorg. Chem.* **2013**, *52* (11), 6617−6626. (b) Su, J.; Li, W.-L.; Lopez, G. V.; Jian, T.; Cao, G.-J.; Li, W.-L.; Schwarz, W. H. E.; Wang, L.-S.; Li, J. Probing the Electronic Structure and Chemical Bonding of Mono-Uranium Oxides with Different Oxidation States: UO_x^- and UO_x (x = 3−5). *J. Phys. Chem. A* **2016**, *120* (7), 1084−1096.

(12) Pyykkö, P.; Lohr, L. L. Relativistically parameterized extended Hueckel calculations. 3. Structure and bonding for some compounds of uranium and other heavy elements. *Inorg. Chem.* **1981**, *20* (7), 1950−1959.

(13) Huang, W.; Xu, W. H.; Schwarz, W. H. E.; Li, J. On the highest oxidation states of metal elements in MO_4 molecules (M = Fe, Ru, Os, Hs, Sm, and Pu). *Inorg. Chem.* **2016**, *55* (9), 4616−4625.

(14) Kato, Y.; Kimura, T.; Yoshida, Z.; Nitani, N. Solid-liquid phase equilibria of Np(VI) and of U(VI) under controlled CO_2 partial pressures. *Radiochim. Acta* **1996**, *74* (s1), 21−25.

(15) Fedosseev, A. M.; Gogolev, A. V.; Charushnikova, I. A.; Shilov, V. P. Tricarbonate complex of hexavalent Am with guanidinium: synthesis and structural characterization of $[C(NH_2)_3]_4[AmO_2(CO_3)_3]\cdot 2H_2O$, comparison with $[C(NH_2)_3]_4[AnO_2(CO_3)_3]$ (An = U, Np, Pu). *Radiochim. Acta* **2011**, *99* (11), 679−686.

(16) Eisenstein, J. C.; Pryce, M. H. L. The electronic structure and magnetic properties of uranyl-like ions. II. Plutonyl. *Proc. R. Soc. London, Ser. A* **1956**, *238*, 31−45.

(17) Eisenstein, J. C.; Pryce, M. H. L. Electronic structure and magnetic properties of the neptunyl ion. *J. Res. Natl. Bur. Stand., Sect. A* **1965**, *69A*, 217.

DOI: 10.1021/acs.inorgchem.7b03277
Inorg. Chem. 2018, 57, 2899−2907

(18) Jiang, N.; Schwarz, W. H.; Li, J. Theoretical studies on hexanuclear oxometalates $[M_6L_{19}]^{q-}$ (M = Cr, Mo, W, Sg, Nd, U). Electronic structures, oxidation states, aromaticity, and stability. *Inorg. Chem.* **2015**, *54* (15), 7171−7180.
(19) Kovacs, A.; Konings, R. J. M.; Gibson, J. K.; Infante, I.; Gagliardi, L. Quantum chemical calculations and experimental investigations of molecular actinide oxides. *Chem. Rev.* **2015**, *115* (4), 1725−1759.
(20) Marcalo, J.; Gibson, J. K. Gas-phase energetics of actinide oxides: An assessment of neutral and cationic monoxides and dioxides from thorium to curium. *J. Phys. Chem. A* **2009**, *113* (45), 12599−12606.
(21) Pyykkö, P.; Li, J.; Runeberg, N. Quasirelativistic pseudopotential study of species isoelectronic to uranyl and the equatorial coordination of uranyl. *J. Phys. Chem.* **1994**, *98* (18), 4809−4813.
(22) Kovács, A.; Konings, R. J. M. Theoretical study of UX_6 and UO_2X_2 (X = F, Cl, Br, I). *J. Mol. Struct.: THEOCHEM* **2004**, *684* (1−3), 35−42.
(23) Liu, J.-B.; Chen, G. P.; Huang, W.; Clark, D. L.; Schwarz, W. H. E.; Li, J. Bonding trends across the series of tricarbonato-actinyl anions $[(AnO_2)(CO_3)_3]^{4-}$ (An = U−Cm): the plutonium turn. *Dalton Trans.* **2017**, *46*, 2542−2550.
(24) Su, J.; Dau, P. D.; Liu, H. T.; Huang, D. L.; Wei, F.; Schwarz, W. H.; Li, J.; Wang, L. S. Photoelectron spectroscopy and theoretical studies of gaseous uranium hexachlorides in different oxidation states: UCl_6^{q-} (q = 0−2). *J. Chem. Phys.* **2015**, *142* (13), 134308.
(25) Fujii, T.; Uehara, A.; Kitatsuji, Y.; Yamana, H. Theoretical and experimental study of the vibrational frequencies of UO_2^{2+} and NpO_2^{2+} in highly concentrated chloride solutions. *J. Radioanal. Nucl. Chem.* **2015**, *303* (1), 1015−1020.
(26) Lan, J. H.; Wang, C. Z.; Wu, Q. Y.; Wang, S. A.; Feng, Y. X.; Zhao, Y. L.; Chai, Z. F.; Shi, W. Q. A Quasi-relativistic density functional theory study of the Actinyl(VI, V) (An = U, Np, Pu) complexes with a six-membered macrocycle containing Pyrrole, Pyridine, and Furan subunits. *J. Phys. Chem. A* **2015**, *119* (34), 9178−9188.
(27) Shamov, G. A. Oxidative nucleophilic substitution of hydrogen in the sapphyrin dioxouranium(VI) complex: a relativistic DFT study. *J. Am. Chem. Soc.* **2011**, *133* (12), 4316−4329.
(28) Wang, Y. L.; Liu, Z. Y.; Li, Y. X.; Bai, Z. L.; Liu, W.; Wang, Y. X.; Xu, X. M.; Xiao, C. L.; Sheng, D. P.; Diwu, J.; Su, J.; Chai, Z. F.; Albrecht-Schmitt, T. E.; Wang, S. Umbellate distortions of the uranyl coordination environment result in a stable and porous polycatenated framework that can effectively remove cesium from aqueous solutions. *J. Am. Chem. Soc.* **2015**, *137* (19), 6144−6147.
(29) (a) Çiçek, B.; Yıldız, A. Synthesis, metal ion complexation and computational studies of thio oxocrown ethers. *Molecules* **2011**, *16* (12), 8670−8683. (b) Huang, W.; Jiang, N.; Schwarz, W. H. E.; Yang, P.; Li, J. Diversity of Chemical Bonding and Oxidation States in MS_4 Molecules of Group 8 Elements. *Chem. - Eur. J.* **2017**, *23*, 10580−10589.
(30) Choppin, G. R. Actinide speciation in the environment. *J. Radioanal. Nucl. Chem.* **2007**, *273*, 695−703.
(31) Rogers, R. D.; Bauer, C. B.; Bond, A. H. Crown-ethers as actinide extractants in acidic aqueous biphasic systems-partitioning behavior in solution and crystallographic analyses of the solid-state. *J. Alloys Compd.* **1994**, *213-214*, 305−312.
(32) Rogers, R. D.; Bond, A. H.; Hipple, W. G.; Rollins, A. N.; Henry, R. F. Synthesis and structural elucidation of novel uranyl crown-ether compounds isolated from nitric, hydrochloric, sulfuric, and acetic-acids. *Inorg. Chem.* **1991**, *30* (12), 2671−2679.
(33) Gokel, G. W.; Leevy, W. M.; Weber, M. E. Crown ethers: Sensors for ions and molecular scaffolds for materials and biological models. *Chem. Rev.* **2004**, *104* (5), 2723−2750.
(34) Gong, Y.; Gibson, J. K. Crown ether complexes of uranyl, neptunyl, and plutonyl: Hydration differentiates inclusion versus outer coordination. *Inorg. Chem.* **2014**, *53* (11), 5839−5844.
(35) Zhou, W.; Sun, X. L.; Gu, L.; Bao, F. F.; Xu, X. X.; Pang, C. Y.; Gu, Z. G.; Li, Z. J. A green strategy for lithium isotopes separation by using mesoporous silica materials doped with ionic liquids and benzo-15-crown-5. *J. Radioanal. Nucl. Chem.* **2014**, *300* (2), 843−852.
(36) Doxsee, K. M.; Wierman, H. R.; Weakley, T. J. R. Unusual coordination number and geometry in a potassium 18-crown-6 complex. *J. Am. Chem. Soc.* **1992**, *114* (13), 5165−5171.
(37) Eller, P. G.; Penneman, R. A. Uranyl nitrate tetrahydrate-18-crown-6 compound, $UO_2(NO_3)_2(H_2O)_2$-$2H_2O$-(18-Crown-6). Non-coordination of uranyl by the crown ether. *Inorg. Chem.* **1976**, *15* (10), 2439−2442.
(38) Mougel, V.; Chatelain, L.; Pecaut, J.; Caciuffo, R.; Colineau, E.; Griveau, J. C.; Mazzanti, M. Uranium and manganese assembled in a wheel-shaped nanoscale single-molecule magnet with high spin-reversal barrier. *Nat. Chem.* **2012**, *4* (12), 1011−1017.
(39) Hu, S.-X.; Li, W.-L.; Dong, L.; Gibson, J. K.; Li, J. Crown ether complexes of actinyls: A computational assessment of $AnO_2(15\text{-crown-}5)^{2+}$ (An = U, Np, Pu, Am, Cm). *Dalton Trans.* **2017**, *46* (36), 12354−12363.
(40) Frisch, M. J.; Trucks, G. W.; Schlegel, H. B.; Scuseria, G. E.; Robb, M. A.; Cheeseman, J. R.; Scalmani, G.; Barone, V.; Mennucci, B.; Petersson, G. A.; Nakatsuji, H.; Caricato, M.; Li, X.; Hratchian, H. P.; Izmaylov, A. F.; Bloino, J.; Zheng, G.; Sonnenberg, J. L.; Hada, M.; Ehara, M.; Toyota, K.; Fukuda, R.; Hasegawa, J.; Ishida, M.; Nakajima, T.; Honda, Y.; Kitao, O.; Nakai, H.; Vreven, T.; Montgomery, J. A., Jr.; Peralta, J. E.; Ogliaro, F.; Bearpark, M.; Heyd, J. J.; Brothers, E.; Kudin, K. N.; Staroverov, V. N.; Kobayashi, R.; Normand, J.; Raghavachari, K.; Rendell, A.; Burant, J. C.; Iyengar, S. S.; Tomasi, J.; Cossi, M.; Rega, N.; Millam, J. M.; Klene, M.; Knox, J. E.; Cross, J. B.; Bakken, V.; Adamo, C.; Jaramillo, J.; Gomperts, R.; Stratmann, R. E.; Yazyev, O.; Austin, A. J.; Cammi, R.; Pomelli, C.; Ochterski, J. W.; Martin, R. L.; Morokuma, K.; Zakrzewski, V. G.; Voth, G. A.; Salvador, P.; Dannenberg, J. J.; Dapprich, S.; Daniels, A. D.; Farkas, O.; Foresman, J. B.; Ortiz, J. V.; Cioslowski, J.; Fox, D. J. *Gaussian 09*, revision C.01; Gaussian, Inc.: Wallingford, CT, 2009.
(41) Baerends, E. J.; Ellis, D. E.; Ros, P. Self-consistent molecular Hartree-Fock-Slater calculations I. The computational procedure. *Chem. Phys.* **1973**, *2* (1), 41−51.
(42) Baerends, E. J. et al. *ADF2013*; SCM Theoretical Chemistry, Vrije Universiteit: Amsterdam, The Netherlands, 2013. http://www.scm.com.
(43) Mulliken, R. S. Electronic population analysis on LCAO−MO molecular wave functions. 1. *J. Chem. Phys.* **1955**, *23* (10), 1833−1840.
(44) Baerends, E. J.; Branchadell, V.; Sodupe, M. Atomic reference energies for density functional calculations. *Chem. Phys. Lett.* **1997**, *265* (3−5), 481−489.
(45) Perdew, J. P.; Ernzerhof, M.; Burke, K. Rationale for mixing exact exchange with density functional approximations. *J. Chem. Phys.* **1996**, *105* (22), 9982−9985.
(46) van Lenthe, E.; Baerends, E. J.; Snijders, J. G. Relativistic regular 2-component hamiltonians. *J. Chem. Phys.* **1993**, *99* (6), 4597−4610.
(47) van Lenthe, E.; Baerends, E. J.; Snijders, J. G. Relativistic total energy using regular approximations. *J. Chem. Phys.* **1994**, *101* (11), 9783−9792.
(48) van Lenthe, E.; Baerends, E. J. Optimized Slater-type basis sets for the elements 1−118. *J. Comput. Chem.* **2003**, *24* (9), 1142−1156.
(49) Klamt, A.; Schüürmann, G. COSMO−A new approach to dielectric screening in solvents with explicit expressions for the screening energy and its gradient. *J. Chem. Soc., Perkin Trans. 2* **1993**, *0* (5), 799−805.
(50) Allinger, N. L.; Zhou, X. F.; Bergsma, J. Molecular mechanics parameters. *J. Mol. Struct.: THEOCHEM* **1994**, *312* (1), 69−83.
(51) Michalak, A.; Mitoraj, M.; Ziegler, T. Bond orbitals from chemical valence theory. *J. Phys. Chem. A* **2008**, *112* (9), 1933−1939.
(52) Versluis, L.; Ziegler, T. The determination of molecular structure by density functional theory. *J. Chem. Phys.* **1988**, *88* (1), 322−328.
(53) Mitoraj, M.; Michalak, A.; Ziegler, T. On the nature of the agostic bond between metal centers and β-hydrogen atoms in alkyl complexes. An analysis based on the extended transition state method

DOI: 10.1021/acs.inorgchem.7b03277
Inorg. Chem. 2018, 57, 2899−2907

and the natural orbitals for chemical valence scheme (ETS-NOCV). *Organometallics* **2009**, *28* (13), 3727−2733.
(54) Nalewajski, R. F.; Mrozek, J. Modified valence indices from the two-particle density matrix. *Int. J. Quantum Chem.* **1994**, *51* (4), 187−200.
(55) Nalewajski, R. F.; Mrozek, J.; Michalak, A. Two-electron valence indices from the Kohn-Sham orbitals. *Int. J. Quantum Chem.* **1997**, *61* (3), 589−601.
(56) Mayer, I. Charge, bond order and valence in the *ab* inition SCF theory. *Chem. Phys. Lett.* **1983**, *97* (3), 270−274.
(57) Michalak, A.; De Kock, R. L.; Ziegler, T. Bond multiplicity in transition-metal complexes: applications of two-electron valence indices. *J. Phys. Chem. A* **2008**, *112* (31), 7256−7263.
(58) Mitoraj, M.; Michalak, A. Natural orbitals for chemical valence as descriptors of chemical bonding in transition metal complexes. *J. Mol. Model.* **2007**, *13* (2), 347−355.
(59) de Silva, P.; Korchowiec, J.; Wesolowski, T. A. Revealing the Bonding Pattern from the Molecular Electron Density Using Single Exponential Decay Detector: An Orbital-Free Alternative to the Electron Localization Function. *ChemPhysChem* **2012**, *13* (15), 3462−3465.
(60) Dolg, M.; Wedig, U.; Stoll, H.; Preuss, H. Energy−adjusted abinitio pseudopotentials for the first row transition elements. *J. Chem. Phys.* **1987**, *86* (2), 866−872.
(61) Cao, X.; Dolg, M.; Stoll, H. Valence basis sets for relativistic energy-consistent small-core actinide pseudopotentials. *J. Chem. Phys.* **2003**, *118* (2), 487−496.
(62) Cao, X.; Dolg, M. Segmented contraction scheme for small-core actinide pseudopotential basis sets. *J. Mol. Struct.: THEOCHEM* **2004**, *673* (1−3), 203−209.
(63) Kendall, R. A.; Dunning, T. H., Jr.; Harrison, R. J. Electron affinities of the first-row atoms revisited. Systematic basis sets and wave functions. *J. Chem. Phys.* **1992**, *96* (9), 6796−6806.
(64) Becke, A. D. Density-functional thermochemistry. 3. The role of exact exchange. *J. Chem. Phys.* **1993**, *98* (7), 5648−5652.
(65) Lee, C. T.; Yang, W. T.; Parr, R. G. Development of the colle-salvetti correlation-energy formula into a functional of the electron-density. *Phys. Rev. B: Condens. Matter Mater. Phys.* **1988**, *37* (2), 785−789.
(66) Gong, Y.; Andrews, L.; Liebov, B. K.; Fang, Z.; Garner, E. B., III; Dixon, D. A. Reactions of Laser−ablated U Atoms with $(CN)_2$: Infrared Spectra and Electronic Structure Calculations of UNC, $U(NC)_2$, and $U(NC)_4$ in Solid Argon. *Chem. Commun.* **2015**, *51* (18), 3899−3902.
(67) Gibson, J. K.; Hu, H.-S.; Van Stipdonk, M. J.; Berden, G.; Oomens, J.; Li, J. Infrared multiphoton dissociation spectroscopy of a gas-phase complex of uranyl and 3-oxa-glutaramide: An extreme red-shift of the $[O=U=O]^{2+}$ asymmetric stretch. *J. Phys. Chem. A* **2015**, *119* (14), 3366−3374.
(68) Reed, A. E.; Curtiss, L. A.; Weinhold, F. Intermolecular interactions from a natural bond orbital, donor−acceptor viewpoint. *Chem. Rev.* **1988**, *88* (6), 899−926.
(69) Reed, A. E.; Weinstock, R. B.; Weinhold, F. Natural−population analysis. *J. Chem. Phys.* **1985**, *83* (2), 735−746.
(70) Krishnan, R.; Binkley, J. S.; Seeger, R.; Pople, J. A. Self−consistent molecular orbital methods. XX. A basis set for correlated wave functions. *J. Chem. Phys.* **1980**, *72* (1), 650−654.
(71) Glendening, E. D.; Badenhoop, J. K.; Reed, A. E.; Carpenter, J. E.; Bohmann, J. A.; Morales, C. M.; Weinhold, F. *NBO* 5.0; Theoretical Chemistry Institute, University of Wisconsin: Madison, WI, 2001.
(72) Alexander, V. Design and synthesis of macrocyclic ligands and their complexes of lanthanides and actinides. *Chem. Rev.* **1995**, *95* (2), 273−342.
(73) Leich, V.; Lamberts, K.; Spaniol, T. P.; Okuda, J. Crown ether adducts of light alkali metal triphenylsilyls: synthesis, structure and hydrosilylation catalysis. *Dalton Trans.* **2014**, *43* (38), 14315−14321.
(74) Pyykkö, P. Additive covalent radii for single-, double-, and triple-bonded molecules and tetrahedrally bonded crystals: A summary. *J. Phys. Chem. A* **2015**, *119* (11), 2326−2337.
(75) Tassell, M. J.; Kaltsoyannis, N. Covalency in $AnCp_4$ (An = Th-Cm): a comparison of molecular orbital, natural population and atoms-in-molecules analyses. *Dalton Trans.* **2010**, *39* (29), 6719−6725.
(76) Li, J.; Bursten, B. E. Bis(arene) Actinide Sandwich Complexes, $(\eta^6\text{-}C_6H_3R_3)_2An$: Linear or Bent? *J. Am. Chem. Soc.* **1999**, *121* (43), 10243−10244.
(77) Shinkai, S. Molecular recognition of calixarene-based host molecules. *J. Inclusion Phenom. Mol. Recognit. Chem.* **1989**, *7* (2), 193−201.
(78) Schnaars, D. D.; Gaunt, A. J.; Hayton, T. W.; Jones, M. B.; Kirker, I.; Kaltsoyannis, N.; May, I.; Reilly, S. D.; Scott, B. L.; Wu, G. Bonding trends traversing the tetravalent actinide series: synthesis, structural, and computational analysis of $An^{IV}(^{Ar}acnac)_4$ complexes (An = Th, U, Np, Pu; ^{Ar}acnac = ArNC(Ph)CHC(Ph)*O*; Ar = 3,5-^{t}Bu$_2$C$_6$H$_3$). *Inorg. Chem.* **2012**, *51* (15), 8557−8566.
(79) Infante, I.; Kovacs, A.; La Macchia, G.; Shahi, A. R. M.; Gibson, J. K.; Gagliardi, L. Ionization energies for the actinide mono- and dioxides series, from Th to Cm: Theory versus experiment. *J. Phys. Chem. A* **2010**, *114* (19), 6007−6015.
(80) Kaltsoyannis, N. Transuranic computational chemistry. *Chem. - Eur. J.* **2017**, DOI: 10.1002/chem.201704445.
(81) Hirshfeld, F. L. Bonded-atom fragments for describing molecular charge-densities. *Theoret. Chim. Acta* **1977**, *44* (2), 129−138.
(82) Swart, M.; Van Duijnen, P. T.; Snijders, J. G. A charge analysis derived from an atomic multipole expansion. *J. Comput. Chem.* **2001**, *22* (1), 79−88.
(83) Shamov, G. A.; Schreckenbach, G. Relativistic density functional theory study of dioxoactinide(VI) and -(V) complexation with alaskaphyrin and related Schiff-base macrocyclic ligands. *J. Phys. Chem. A* **2006**, *110* (30), 9486−9499.

DOI: 10.1021/acs.inorgchem.7b03277
Inorg. Chem. 2018, 57, 2899−2907